JOURNAL OF MATERIALS SCIENCE **40** (2005) 5741–5749

# Formation of strong ceramified ash from silicone-based compositions

J. MANSOURI*, R. P. BURFORD
*School of Chemical Engineering and Industrial Chemistry, University of New South Wales, NSW 2052, Australia; Cooperative Research Centre for Polymers, 32 Business Park Drive, Nothing Hill, Victoria 3168, Australia*
*E-mail: j.mansouri@unsw.edu.au*

Y. B. CHENG, L. HANU
*School of Physics and Materials Engineering, Monash University, Victoria 3800, Australia; Cooperative Research Centre for Polymers, 32 Business Park Drive, Nothing Hill, Victoria 3168, Australia*

**Published online:** 25 August 2005

Compared with many other polymers, polysiloxanes have shown some desirable properties on fire. These include a slow burning rate without a flaming drip and low emissions of non-toxic smoke. However, the residue formed by firing silicones in air is powdery and has little strength for structural use. Addition of certain inorganic fillers into silicone base polymers can improve the ceramic strength, leading to ceramics with good integrity and shape retention after firing. In this work, compositions based on silicate filled silicone polymers were made and their properties were explored. An insight into the mechanism of the ceramic formation after firing at temperatures up to 1050°C was obtained. Techniques including field emission scanning electron microscopy (FESEM) and transmission electron microscopy (TEM) were used to observe microstructure and phase development. Thermal stability was studied by thermogravimetric analysis (TGA) and differential thermal analysis (DTA). A mechanism for formation of a strong and coherent ceramic is proposed. 

## 1. Introduction

Polyorganosiloxanes are heat resistant polymers that are widely used in the production of systems that operate at high temperatures. These polymers comprise a polymer backbone of silicon and oxygen atoms, the silicon atoms carrying two organic side groups, examples being methyl, vinyl, and phenyl or fluoroalkyl moieties. Vulcanisation converts the silicone rubber into articles of high heat resistance, good electrical insulating properties and good low temperature stability.

There are many approaches to improve fire and flame performance of polymers. Inorganic fillers such as aluminium trihydrate (ATH) and magnesium hydroxide ($Mg(OH)_2$) [1] lower the combustibility of organic polymers by endothermic dehydration reactions. It is also reported that zinc borate can have a synergistic effect in polyolefin/ATH and polyolefin/$Mg(OH)_2$ flame retardant formulations [2]. In this case ATH or $Mg(OH)_2$ formed a ceramic-like barrier on the surface of polymer. Other fillers such as $TiO_2$ form a non-combustible, noncarbon barrier layer [3, 4], this protects the underlying polymer from incoming heat flux and reduces combustible species available as fuel in the gas phase. The flame retardant mechanism for typical halogenated materials is achieved by release of combustion gases that form a protective gaseous layer around the flame. However these combustion gases are the main reason for the dense smoke and corrosive nature of these materials while burning.

Silicone-based flame retardant systems offer an environmentally safer alternative to halogenated fire retardants. Siloxane polymers have been shown to possess desirable fire performance properties in comparison to most organic polymers [5]. Benrashid and Nelson [6] reported that polyurethanes modified with silicone had improved chemical and thermal resistance, and that flammability depends on systems being developed where the highest level of silicone is at the surface. Fire retardancy is thought to be due to surface silica insulating and protecting the bulk from oxidation. Unlike most organic polymers, silicones do not burn completely, but form a powdery silica ash layer on top of the polymer. It serves as an "insulating blanket", by reducing the amount of pyrolysis by-products available for burning into the gas phase and by delaying the volatilisation of decomposed

*Author to whom all correspondence should be addressed.
0022-2461 
DOI: 10.1007/s10853-005-1427-8

products [7]. However the silica residue obtained by firing silicone polymer alone has a powdery form and is far too weak for any useful structural applications.

The microstructure strongly affects ceramic strength and coherence, and so some additives can improve flame retardancy by changing ceramic morphology. Weil *et al*. [8] found that iron compounds can behave as effective flame retardants in certain polymers by altering morphology with ceramics being shiny, continuous and free of cracks. While the mechanism is uncertain, a catalytic effect might be responsible [9]. A known catalytic additive is platinum which has been used at low levels in peroxide-cured silica filled silicone rubbers [10]. Again, details are not clear, although a French study suggests that it might inhibit depolymerisation of the siloxane structure [11]. Hayashida *et al* [12] suggests that thermal decomposition of silicone rubber is suppressed by the formation of cross-linked structures. This class of compounds is one of the most efficient flame-retardant additives known, having a detectable effect at parts per million levels.

Ceramifying polymer-ceramic composites that possess desirable performance of the polymer at room temperature as well as those of a ceramic at elevated temperatures would be useful in many applications. Fire-retarding additives that promote char formation during burning to reduce polymer flammability have also been investigated [13, 14]. Char formation is seen as an effective way of reducing flammability of polymer based materials since it acts as a barrier to both thermal and mass transport [15].

In this work compositions based on silicone/silicate filler were made and their microstructure and thermal properties studied. Changes in phase behaviour were also carried out using XRD, leading to a mechanism for ceramic formation.

## 2. Experimental

### 2.1. Materials

All materials were used as received.

Two different types of silicone polymers were used in this work. NPC 80 is a silicone gum supplied by Dow Corning and Elastosil R401/80S is a silicone gum from Wacker-Chemie. Properties of these rubbers are given in Table I. NPC 80 is filled with about 40 wt% silica according to supplier data sheet.

Dicumyl peroxide (Di-Cup 40C, cure temperature range: 160–170°C; Akzo-Nobel) in powder form was used as the curing agent.

TABLE I Properties of silicone rubbers

| | NPC 80[c] | R401/80S |
|---|---|---|
| Density, (g/cm)[b] | 1.43 | 1.17 |
| Hardness, Shore A unit[b] | 79—89 | 75–85 |
| Glass transition, (°C)[a] | −118 | −122 |
| Cold crystallisation, (°C)[a] | −93 | −80 |
| Melting point, (°C)[a] | −41 | −39 |

a: measured by DSC.
b: From suppliers catalogues.
c: Silica-filled according to supplier.

TABLE II Specifications of muscovite mica used in this study

| Product code | Particle size, ($\mu$m) | Description | Supplier |
|---|---|---|---|
| GA100 | 114 | Dry ground muscovite mica flake | Commercial Minerals Pty. Ltd. (Australia) |

TABLE III Major components of mica in terms of elemental oxide (XRF)

| Oxide | GA100 |
|---|---|
| $SiO_2$ | 46 |
| $Al_2O_3$ | 33 |
| $K_2O$ | 10 |
| $Fe_2O_3$ | 5 |
| $Na_2O$ | 0.6 |
| MgO | 0.6 |

TABLE IV Compounds formulations (g)

| | Composition code | |
|---|---|---|
| Components | SNG20 | SWG20 |
| NPC 80 | 80 | – |
| Elastosil R401/80S | – | 80 |
| Mica GA100 | 20 | 20 |
| DCP | 1.44 | 1.44 |

A muscovite mica (alkali alumino-silicate), GA 100, was used as filler (Table II). It is expected that the alkali component of mica facilitates glass formation in the ceramic formed after firing of rubber composites. The chemical composition of GA100 is given in Table III.

### 2.2. Sample preparation

All compounds were prepared using a conventional two-roll mill, with silicone rubber first softened at room temperature then fillers were mixed in until a homogeneous batch was obtained. The curing agent was then added and processed until a visually good dispersion was achieved. Compounds were moulded and cured into flat sheets by compression moulding at 180°C for 20 min under 10 MPa pressure. Symbols and related formulations of compounds used in this study are summarised in Table IV.

### 2.3. Sample pyrolysis

Pyrolysis of flat sheet samples (50×14×2 mm) was performed using a muffle furnace at different temperatures with a heating rate of 10–12 °C/min, and was carried out either in nitrogen or air. Cables were burned in a gas furnace according to AS/NZS 3013:1995 (heating to 1050°C and then spraying with water within 30 min).

### 2.4. Characterisation

#### *2.4.1. Thermal characterisation*

(a) *Thermal transitions of silicone*. Glass transitions, crystallisation and melting points of raw rubbers were determined using a 2010 Differential Scanning Calorimeter (TA Instruments). Samples was cooled

from room temperature to –160°C and then heated to 250°C at a heating rate of 20°C/min. Differential thermal analysis was used to study the thermal transitions at temperatures above 500°C, with a Setaram TGA 24 Simultaneous DT/TGA at a heating rate of 10°C/min.

(b) *Mass loss and thermal stability*. The weight loss behaviour of different samples (room temperature to 1050°C) was studied using a TA Instruments 2950 Hi-Resolution thermogravimetric analyser (TGA). In this study, air, nitrogen and 4% oxygen (in nitrogen) were used as furnace atmospheres, the latter was chosen in an attempt to replicate the conditions in a gas fired furnace used in testing the cable samples according to Australian Standard, AS/NZS3013:1995.

#### 2.4.2. X-ray diffraction analysis (XRD)

Wide angle X-ray scattering was conducted using a Philips PW1830 generator with a 371 mpd control. The scan was conducted from a $2\theta$ angle of 2° to 60° at a scan rate of 1°/min.

#### 2.4.3. X-ray fluorescence (XRF)

Chemical compositions of mica was analysed by the X-ray Fluoroscence method using a Philips PW2400 XRF spectrometer. Glass sample disk (40 mm diameter) was prepared using a mixture of flux (borate glass and ammonium nitrate) and sample in the approximate ratio of 5.43:1. The mixture was heated in a platinum-gold crucible for 15 min at 1050°C until the specimen was dissolved. The melt was poured into a graphite disc which was held on a hot plate at about 220°C. An aluminium plunger was then brought down gently to mould and quench the melt [16].

#### 2.4.4. Morphological studies

*(a). FESEM*. Field emission scanning electron microscopy (FESEM) observations of polymer fracture surfaces after immersion in liquid nitrogen, and the surfaces and cross-sections of ceramified ashes embedded in epoxy resin, were made using a Hitachi S4500II instrument. Samples were sputter coated with either gold or carbon using a Polaron Sputter coater unit.

*2. FETEM*. A Philips CM200 field emission transmission electron microscope (FETEM) was used to observe the morphological characteristics of the composites. This instrument allows very high resolution images to be obtained from thin, electron transparent sections of materials. Composite samples were cryomicrotomed (70–100 nm thick sections) at −120°C with a diamond knife using a Leica Ultracut S microtome Unit with FCS cryochamber. The sections were transferred to 200 mesh carbon-coated copper grids. Sucrose solution was used to support the specimen. The intrinsic contrast between mica and the polymer phase was sufficient for imaging, so heavy metal staining of sections prior to imaging was not required.

#### 2.4.5. Flexural strength measurements

The flexural strength of pyrolysed samples was determined by the three-point bend method using an Instron Universal Testing Machine. Samples measuring 50×14×3 mm were fired at various temperatures and held at the target temperature for 30 min. Loads were applied at a rate of 0.5 mm/min. Flexural strength was calculated using Equation 1:

$$S = \frac{3PL}{2bd^2}$$

where $P$ is the maximum load (N), $L$ is the outer support span (mm), $b$ is the specimen width (mm) and $d$ is the specimen thickness (mm), to give S in MPa.

#### 2.4.6. Cone calorimetry

The cone calorimeter apparatus and test method (ASTM E1354-90) was used for evaluating the flammability of the materials. Specimens (10×10×0.5 cm) were tested using an incident heat flux of 50 kW/m$^2$, allowing the measurement of time to ignition (TTI) and peak heat release rate (PHRR). Specimens were tested in the horizontal orientation. The test method is based on the principle of oxygen consumption calorimetry, where the primary measurements are oxygen concentration and flow rate in the exhaust stream. The heat flux used represents moderate to severe fire test conditions. Under exposure to the radiant heat conditions, ignition of the specimens is accomplished with a high-voltage spark igniter.

## 3. Results and discussion

### 3.1. Microstructure of the unfired composite

Fig. 1 shows the morphology of freeze fracture sections of a composite consisting 80 wt% silicone rubber (NPC 80) and 20 wt% of muscovite mica GA100 (Composition SNG20 in Table IV).

Dispersion of mica plates in the polymer matrix was aligned and adhesion between mica and matrix was good. The tensile strength of the silicone rubber containing the mica was 30% lower (i.e. 4.5 vs. 6.3 MPa) than the silicone rubber, due mainly to the large particle

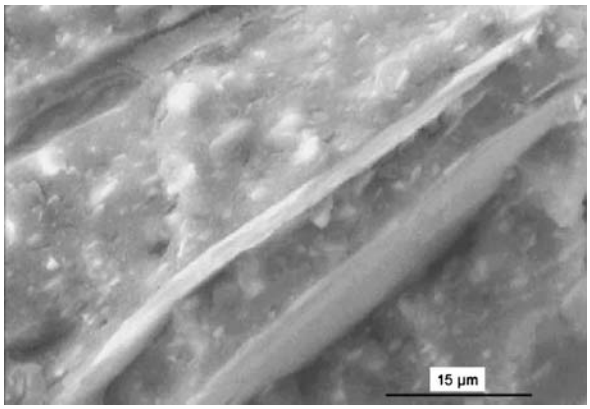


*Figure 1* Scanning electron micrograph for a fracture cross section of SNG20.

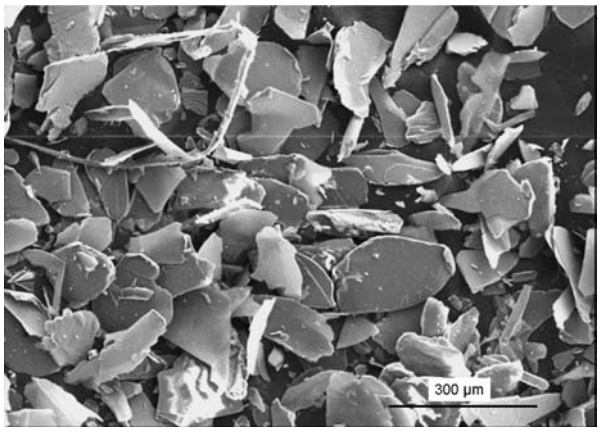


*Figure 2* Scanning electron micrograph for muscovite mica GA100 plates.

size of the mica flakes (Fig. 2). The mica plates are platy, with irregular and sharp boundaries, and have lengths from 100–300 $\mu$m as shown in Fig. 2 for the GA100 type. Fig. 1 also shows small and nearly round particles dispersed uniformly in the matrix, these being silica particles that are in the NPC 80 rubber to provide reinforcement. Considering the density for this rubber (Table I) and the densities for unfilled silicone rubber and silica, the content of silica was calculated to about 40%.

TEM images of a thin section (~50 $\mu$m) of sample SNG20 are shown in Fig. 3. Since the mica particles are composed of heavier elements (Si, Al and K) than carbon, they appear darker in these bright field images. Mica plates about 1 $\mu$m thick (Fig. 3a), are uniformly dispersed in the silicone rubber matrix. Al and K mapping by TEM-EDAX showed that the dark areas are rich in these elements, confirming that these dark areas are mica particles. At higher magnification (Fig. 3b) TEM shows 20–40 nm silica particles homogeneously dispersed in the silicone matrix. Fig. 3a also shows that some of primary mica particles have broken down to smaller particles during mixing and processing.

## 3.2. Thermal stability studies

TGA was performed to determine the maximum decomposition temperature and amount of residue remaining following pyrolysis. The amount of residue is also a good indication of fire performance properties.

Typical TG and DTG curves obtained in a 4% oxygen (in nitrogen) atmosphere for composition SWG20 and the silicone rubber are shown in Fig. 4. The temperature for maximum rate of mass loss and the mass retained increased (20°C and 12%, respectively) by the addition of mica, indicating improvement in thermal stability. Residues for filled compounds were strong, with quite good dimensional stability while those remaining from unfilled samples were weak and powdery. Similar results were observed for compounds based on silicone rubber from Dow Corning (NPC 80).

Thermal oxidative degradation of compounds in air gives results that are quite different to those obtained using 4% oxygen. There are at least two stages of degradation (Fig. 5). The first stage takes place at a much

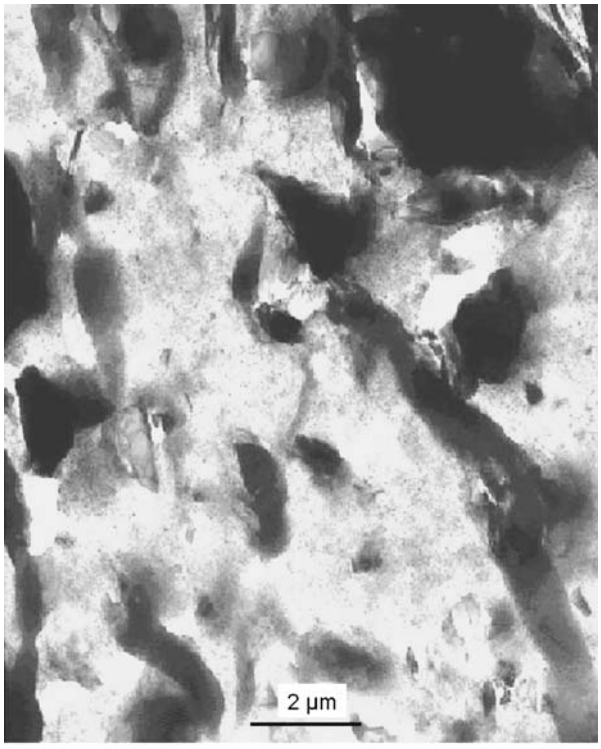


(a)

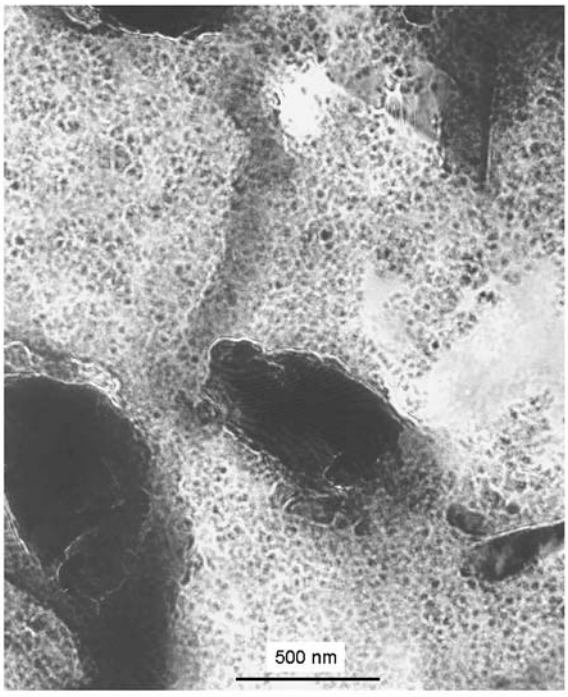


(b)

*Figure 3* TEM images of NPC80/mica GA100 composite (SNG20 composition).

lower temperature in air than in the 4% oxygen environment (see also Table V). For PDMS it is reported that the major degradation products are a mixture of volatile cyclic dimethyl siloxane, $CO_2$, water and $SiO_2$ [17]. The lower $T_{max}$ might be due to the higher concentration of oxygen catalysing the depolymerisation reaction of PDMS to volatile cyclic oligomers. Comparison of thermal traces for filled and unfilled samples showed that both thermal stability, and the residue in air, increased with added filler. The reason for the improvement in the thermal stability of filled silicone rubber

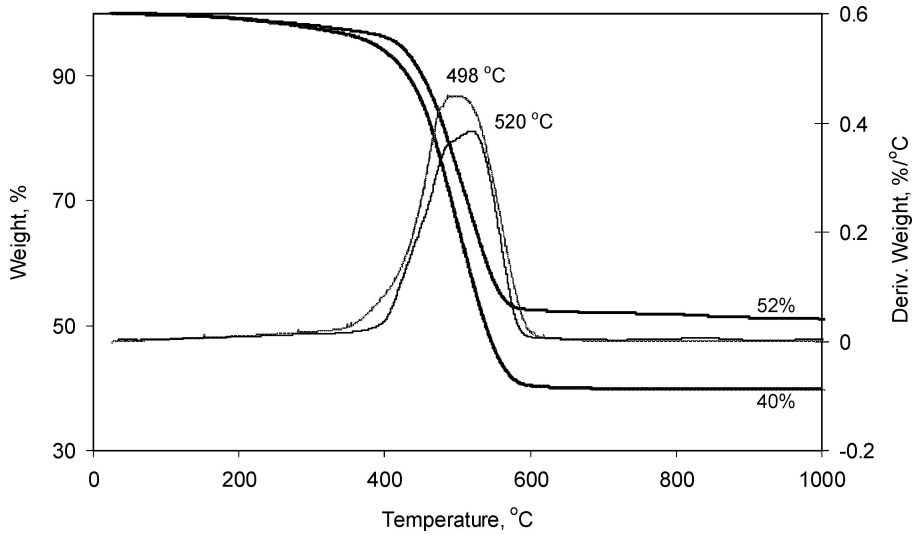


*Figure 4* TG and DTG curves of Wacker R401/80s gum and composition SWG20 compound in 4% oxygen.

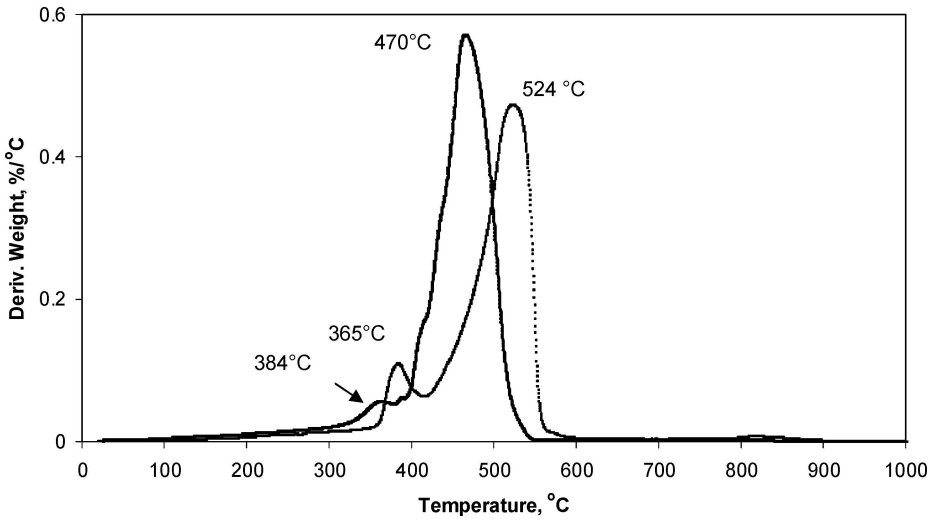


*Figure 5* DTG curves of Wacker R401/80s gum (*left*) and Composition SWG20 (*right*) in air.

is probably due to blocking of active centres for initiation of degradation and the promotion of crosslinking points. Another possibility is the reduction of transport rate of thermal degradation products through the molten polymer layer due to an increase in melt viscosity from the reaction of filler with polymer decomposition products. Residues for both filled and unfilled samples were more brittle in this environment, as compared with 4% oxygen environment. The amount of residue in air is slightly higher, probably due to the presence of more oxidised products.

TABLE V Thermal characteristics of different compounds by TGA and DTG in 4% oxygen and in air (figures in brackets)

| Sample | Onset of deg. (1% weight loss), (°C) | Temperature for maximum rate of mass loss, (°C) | Percentage of residue at 1050°C (%) |
|---|---|---|---|
| NPC80 gum | 300 (300, 420) | 498 (393, 504) | 57 (62) |
| SNG20 | 300 (300, 450) | 522 (416, 531) | 66 (67) |
| Wacker R401/80s gum | 300 (300, 400) | 498 (366, 466) | 40 (52) |
| SWG20 | 300 (300, 420) | 520 (384, 524) | 52 (57) |

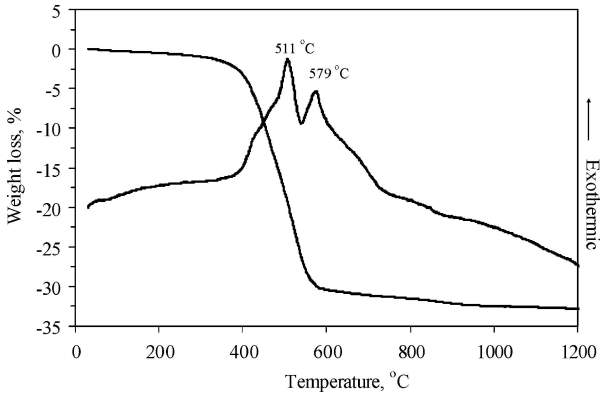


*Figure 6* DTA/TGA trace for composition SNG20 in 4% oxygen atmosphere in nitrogen.

DTA/TGA analysis was conducted on composition SNG20 to study the thermal transitions at temperatures above 500°C.

The DTA traces in an oxygen depleted environment showed two exothermic peaks at 511°C and 579°C

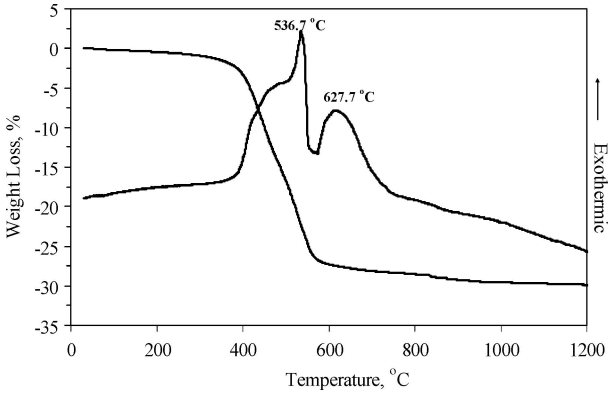


*Figure 7* DTA/TGA analysis of composition SNG20 in air.

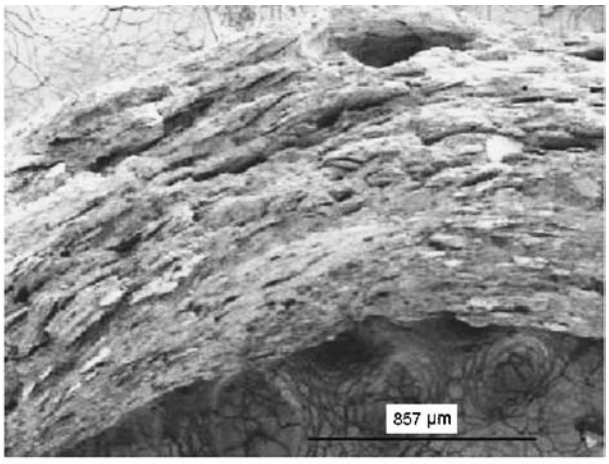


(a)

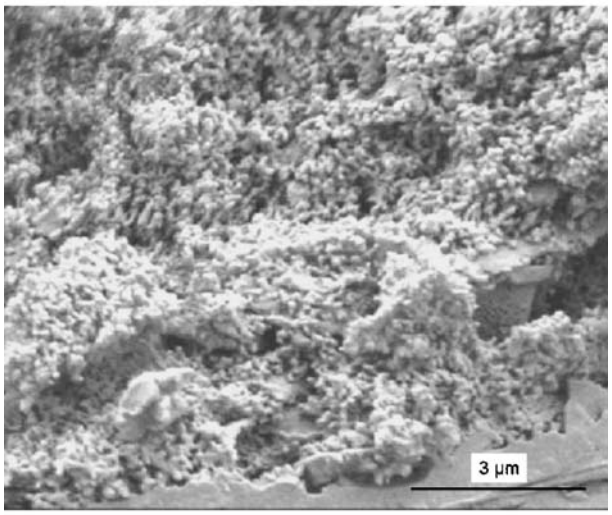


(b)

*Figure 8* Scanning electron micrograph of cross-section of SNG20 insulation layer after firing at 1050°C at (a) low and (b) high magnifications.

(Fig. 6). The first peak was in the same temperature range where the major weight loss occurred. When the sample was pyrolysed in air (Fig. 7) these exothermic peaks shifted to higher temperatures (537 and 627°C). Other workers studying the thermal characteristics of polysiloxanes reported the presence of exothermic peaks at a similar range of temperatures. For example, an exothermic peak at 530°C for polydiphenyl siloxane [18] and a broad exothermic for PDMS between 200-600°C [19] have been reported. These exothermic reactions were related to the deterioration of the main polymer chain. The second exothermic peak, and also the shoulder at the higher temperature, may be due to the dehydration and decomposition of mica. TGA traces for mica GA100 showed a weight loss of 4% when temperature raised from 600 to 900°C.

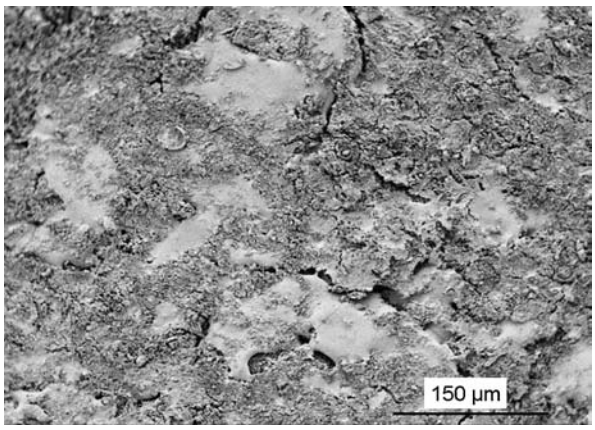


*Figure 9* Scanning electron micrograph of the outer surface of cable after fire test.

*Fire Performance*. Silicone-based polymers exhibit good fire performance properties in terms of both time to ignition and rate of heat release when compared to most organic polymers.

The time to ignition (TTI) for silicone, when the heat release rate in calorimeter reaches 50 kW/m$^2$, is 75 s (Table VI). Upon addition of muscovite, the TTI is increased and the peak rate of heat release is decreased, a trend indicating an improvement in fire performance. As a result, muscovite-filled silicone offers some improvement in fire performance.

### 3.3. Microstructure of ceramified ash

To evaluate fire performance properties, a test single-core cable was insulated with composition SNG20 (Table IV). The thickness of insulation layer was 1.7 mm and no outer sheathing layer was used. This cable was fired in air to 1050°C and maintained at maximum firing temperature for 30 min, then sprayed with a water jet (Fire test conditions for cables according to Australian Standard, AS/NZS3013:1995). Upon firing, the cable formed a strong ceramic with no visible cracks. The residue was a coherent and strong ceramic that was able to withstand small mechanical shocks from the water spray applied at the end of firing. Ceramic

TABLE VI Effects of mica on fire performance of silicone polymer based composites

| Compound | Time to ignition TTI (s) | Peak rate of heat release (kW/m$^2$) |
|---|---|---|
| Silicone | 75 | 144 |
| Silicone + 20 wt% mica | 92 | 98 |

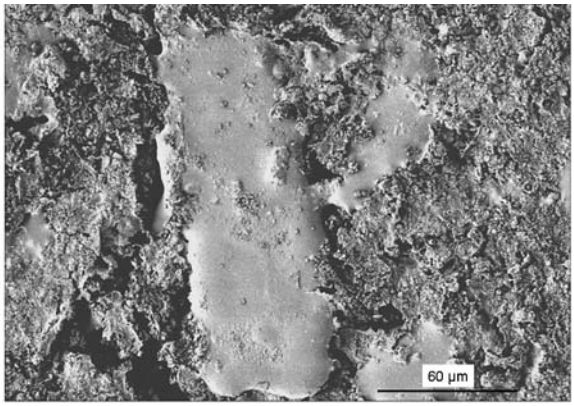


(a)

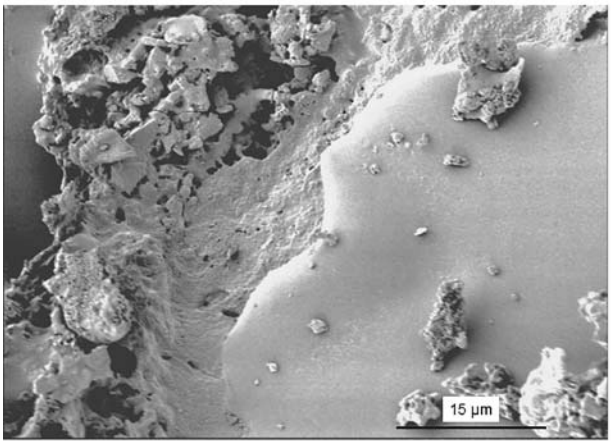


(b)

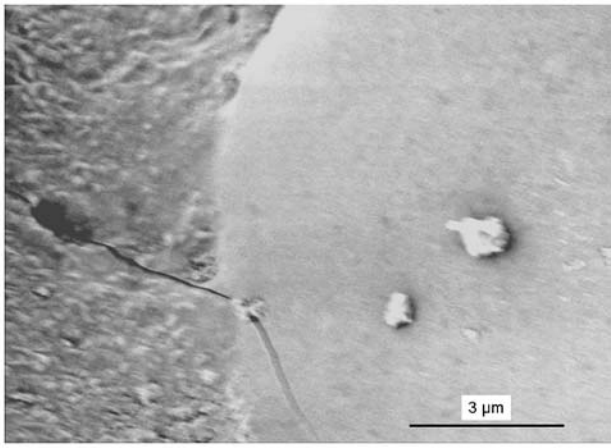


(c)

*Figure 10* Surface morphology of the top layer of the SNG20 insulation after the AS/NZS 3013: 1995 fire test at different magnifications.

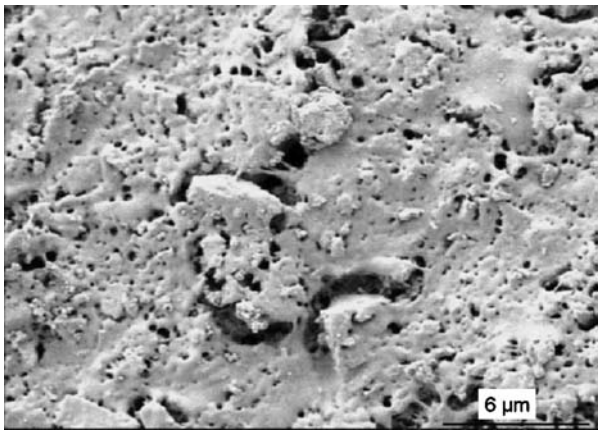


*Figure 11* Scanning electron micrograph of the inner side of the SNG20 insulation layer after the fire test.

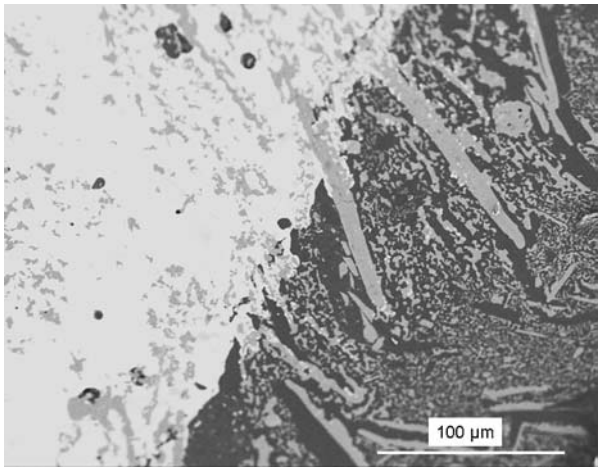


*Figure 12* Scanning electron micrograph of a cross section of cable showing the interaction between mica particles and copper. Bright area is conductor and grey area is ceramified insulation.

microstructure was studied by FESEM to determine the reason for the high strength and integrity displayed by this particular specimen. Microstructure analysis revealed mica plates and the matrix in the cable insulation had formed a multi-layer structure (Fig. 8a). The continuous phase is mainly silica derived from silicone rubber pyrolysis and is dense, with pores as small as 30 nm, as shown in Fig. 8b.

Fig. 9 shows the outer surface of the cable, with the shape of mica plates at the edges clearly being altered after heating to 1050°C (see Fig. 2 for comparison).

At higher magnification (Fig. 10a and b) evidence for edge melting and joining of mica plates is shown. This results from eutectic reactions at the interfaces between the mica particles and silica formed from decomposition of the silicone polymer matrix. Ordinarily, silicon dioxide and mica each have melting points well above 1050°C. However, when mica ($KAl_2(Si_3AlO_{10})(OH)_2$)

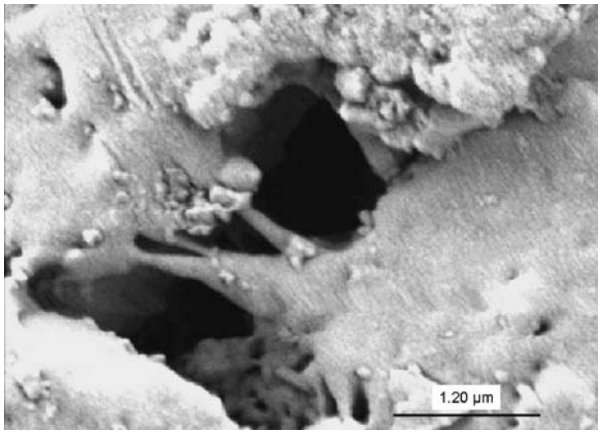


*Figure 13* Scanning electron micrograph showing the formation of microbridges.

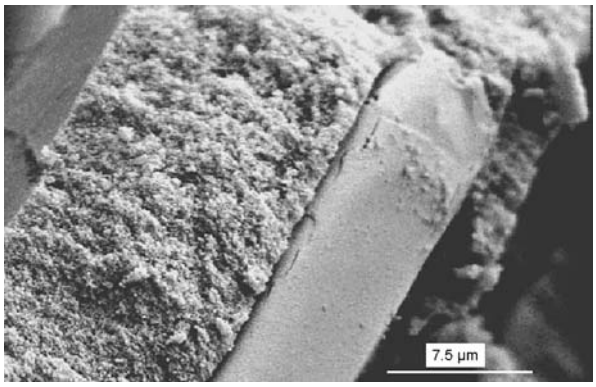


*Figure 14* Scanning electron micrograph of a cross-section of a flat sheet made of SNG20 after heating at 650°C.

decomposes and reacts with silica on heating, a eutectic can form at the interface around 900°C [20]. This eutectic liquid is believed to infiltrate the silica matrix and so act as a bridge between the silicone dioxide particles and the mica particles, giving a coherent structure at the firing temperature. Alkali oxides such as $Na_2O$, LiO and $K_2O$ have been reported to act as flux for $SiO_2$ [21]. Fig. 10b and 10c show evidence of a dense region around the periphery of the mica plates due to the formation of the eutectic liquid phase. This region is up to 5–10 $\mu$m thick.

The inner surface of the cable insulation, which is in contact with the copper conductor, has formed a more liquid phase (Fig. 11). This may be due to the presence of copper or copper oxide which may lower the eutectic temperature. Fig. 12 shows the cross section of a cable after testing and shows evidence of reaction between the copper and ceramic at the interface. The XRD spectrum for the residue remaining after the fire test showed the presence of cuprite species. The diffusion of copper oxides towards the insulation layer has previously been observed by Henrist *et al*. for a cable sheathed with a zinc-borate filled composition [22].

A higher magnification image (Fig. 13) shows the presence of microbridge filling pores, which should improve ash strength. Mica and Wollastonite have been reported to play a similar role for thermoplastics [3, 4].

We believe this microstructure characteristic has led to a stronger ceramic. SWG20 has a flexural strength of about 3.2 MPa while the strength for composition with no filler was too weak to be measurable. When a flat sheet made with the same composition was heated at 650°C, no evidence of local melting of mica plates or liquid phase formation was found, resulting in lower strength for these samples (Fig. 14).

The mechanism of ceramification of the insulation is depicted schematically in Fig. 15.

## 4. Conclusions

We have identified certain mineral fillers from the alkali aluminium silicate group of micas interact with decomposing silicone polymers at elevated temperatures to form strong residue. FESEM analysis demonstrates the local melting of filler particles and bridging between mica and silica particles originating from polymer pyrolysis. These studies lead to the hypothesis that the filled composition forms a coherent and strong residue after exposure to elevated temperatures, as a result of materials of lower melting point, which may be eutectic mixtures, forming at the interface of the alkali aluminium silicate with pyrolysis products.

## Acknowledgements

Measurements of cone calorimetry data by S. Russo (DSTO) and DTA/TGA data by **D.** Cassidy (ANSTO) is gratefully acknowledged.

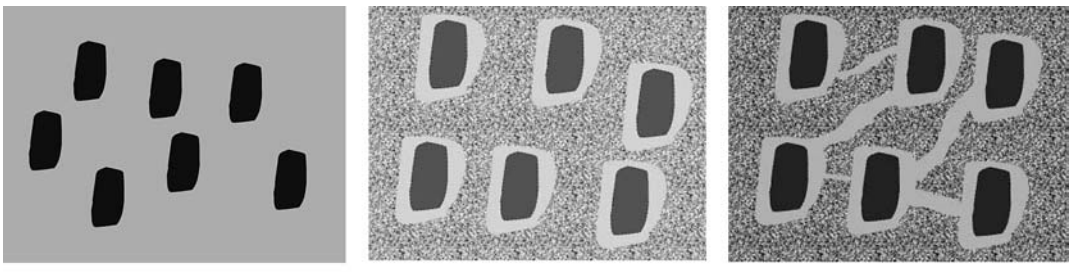


*Figure 15* Schematic presentation of the mechanism of ceramification; (a) rubber-mica composite at room temperature, (b) local melting of mica particles around 800–900°C, (c) bridging above 900°C.

## References


1. J. WANG, J. F. TUNG, M. Y. AHMAD FUAD and R. J. HORNBY, *J. Appl. Polym. Sci.* **60**(9) (1996) 1425.
2. S. BOURBIGOT, M. LE BRAS, R. LEEUWENDAL, K. K. SHEN and D. SCHUBERT, *Polym. Deg. Stab.* **64** (1999) 419.
3. D. SCHARF, Intumescent fire retardants for plastics. (1992) 159 in Papers from Fire Retardant Chemical Association. Fall Conference, Lancaster, Pennsylvania: Fire Retardant Chemical Association.
4. C. E. ANDERSON, J. DZIUK, W. A. MALLOW and J. BUCKMASTER, *J. Fire Sci.* **3** (1985) 161.
5. T. C. CHAO, G. T. BURNS, D. E KATSOULIS and W. C. PAGE. in 42nd International SAMPE Symposium May 1997.
6. R. BENRASHID, G. L. NELSON and W. R. WADE, *J. Appl. Polym. Sci.* **49**(3) (1993) 523.
7. G. MAROSI, A. MÁRTON, P. ANNA, G. BERTALAN, B. MAROSFÖI and A. SZÉP, *Polym. Deg. Stab.* **77** (2002) 259.
8. E. D. WEIL, N. G. PATEL and R. M. LEUWENDAL, Flame retardant polyamide, U.S. Patent 5071894, (1991).
9. R. KAMMERECK, M. NAKAMIZO and P. L. WALKER JR., *Carbon* **12**(3) (1974) 281.
10. M. R. MACLAURY, *J. Fire Flamm.* **10** (1979) 175.
11. R. LAGARDE and J. LAHAYE, *Eur. Polym. J.* **13** (10) (1977) 769.
12. K. HAYASHIDA, S. TSUGE and H. OHTIANI, *Polymer* **44** (2003) 5611.
13. B. MILLER, *Plastics World.* **48** (1990) 48.
14. J. W. GILMAN, *Fire Mate.* **21** (1997) 23.
15. *Idem.* in Proceedings of ADDITIVES '98 Meeting Orlando (1998).
16. K. NORRISH and J. T. HUTTON, *Geochimica et Cosmochimica*, **33** (1969) 431.
17. G. CAMINO, S. S. LOMAKIN and M. LAZZARI, *Polymer* **42** (2001) 2395.
18. L. JAVANOVIC, N. GOVEDARICA, P. R. DVORNIC and I. G. POPOVIC, *Polym. Deg. Stab.* **61** (1998) 87.
19. S. ZULFIQAR and S. AHMA, *ibid.* **71**(2) (2001) 299.
20. B. F. OSBORN and A. MUAN, Fig. 407 in "Phase Equilibrium Diagrams of Oxide Systems," Plate 5, pub. by the Am. Ceram. Soc. and the Edward Orton Jr. Ceramic Foundation, 1960.
21. H. OSCH and K. RICKMANN, *Ceram. Forum-Int.* **67**(4) (1990) 157.
22. C. HENRIST, A. RULMONT, R. CLOOTS, B. GILBERT, A. BERNARD and G. BEYER, *Mater. Lett.* **46**(2/3)(2000) 160.



*Received 25 November 2004*
*and accepted 8 April 2005*